

UNIVERSIDAD DE CONCEPCIÓN



CENTRO DE INVESTIGACIÓN EN  
INGENIERÍA MATEMÁTICA (CI<sup>2</sup>MA)



Asymptotic model for finite-element calculations of diffraction  
by shallow metallic surface-relief gratings

AKHLESH LAKHTAKIA, PETER MONK,  
CINTHYA RIVAS, RODOLFO RODRÍGUEZ,  
MANUEL SOLANO

PREPRINT 2016-22

SERIE DE PRE-PUBLICACIONES



# Asymptotic model for finite-element calculations of diffraction by shallow metallic surface-relief gratings

Cinthya Rivas<sup>1</sup>, Manuel E. Solano<sup>1</sup>, Rodolfo Rodríguez<sup>1</sup>, Peter B. Monk<sup>2</sup>, and A. Lakhtakia<sup>3</sup>.

<sup>1</sup>*CPMA and Departamento de Ingeniería Matemática, Universidad de Concepción, Chile.*

<sup>2</sup>*University of Delaware, Department of Mathematical Sciences, Newark, Delaware 19716, USA.*

<sup>3</sup>*The Pennsylvania State University, Department of Engineering Science and Mechanics, Nanoengineered Metamaterials Group, University Park, PA 16802, USA*

## Abstract

We have formulated an asymptotic model for implementation in the finite element method to calculate diffraction from a planar multilayered structure having a shallow surface-relief grating. The thin grating layer containing the shallow grating is replaced by a planar interface with transmission conditions that differ from the standard continuity conditions. The parameters defining the shallow surface-relief grating are thereby removed from the geometry to the transmission conditions, thereby speeding up finite-element calculations as a very fine mesh is not needed for the thin grating layer. This will considerably reduce the computational cost of optimizing the grating shape, since there is no need to re-mesh at every optimization step.

## 1 Introduction

A surface-relief grating is a momentum adder or subtractor, by virtue of the Floquet–Bloch theorem [1, 2, 3]. To the momentum of an incident plane wave, the grating can add (or subtract) discrete amounts of momentum parallel to the mean plane of the grating, thereby coupling the incident plane wave to either nonspecularly reflected/transmitted plane waves that transport energy away from the grating [4] and/or surface waves whose propagation is guided by the mean plane of the grating [5]. Accordingly, surface-relief gratings are used to reflect or transmit light in nonspecular directions [4, 6] and launch surface waves for optical sensing of analytes [7] as well as to harvest solar energy [8, 9], among other applications.

The discrete amounts of momentum that can be added or subtracted depend on the period  $L$  of the grating as well as the free-space wavelength  $\lambda_0$  of the incident light. While the corrugation depth  $\delta$  of the grating plays an important role in how the addition or subtraction process occurs without violation of the principle of conservation of energy, even corrugation depths that are a small fraction of  $\lambda_0$  can be effective in the excitation of surface waves and enhancement of optical absorptance [10, 11].

Optimal design of a surface-relief grating for a specific application requires the use of rapid and accurate solvers for the frequency-domain Maxwell equations. The optimization process is computationally expensive since these equations must be repeatedly solved for a wide range of optical and geometrical parameters [9, 12]. Several numerical techniques have been formulated to solve the frequency-domain

Maxwell equations in structures containing surface-relief gratings. These numerical techniques include the exact modal method [13], the finite-difference time-domain method [14, 15], and the method of moments [16, 17, 18]. Nowadays, the most commonly used numerical techniques for grating analysis are the rigorous coupled-wave approach (RCWA) [19, 20, 21, 22] and the finite element method (FEM) [23, 12]. The electromagnetic field phasors are expanded in the RCWA in Fourier series with respect to the direction(s) of periodicity, whereas space is discretized through a mesh in the FEM. Even though both the RCWA and the FEM have advantages and disadvantages [25, 24], the FEM is ideally suited for complicated geometries.

A 1D surface-relief grating is commonly specified as the interface  $z = g(x) = g(x \pm L)$  of two dissimilar media. The representation of fields inside the grating layer  $\min_x \{g(x)\} < z < \max_x \{g(x)\}$  of thickness  $\delta = \max_x \{g(x)\} - \min_x \{g(x)\} > 0$  has been a topic of research ever since the time of Rayleigh [26, 27, 28, 29]. An FEM solver can be computationally expensive when the grating layer is electrically thin (i.e.,  $\delta/\lambda_0 \ll 1$ ), because an extremely fine mesh is needed to adequately resolve a thin geometric feature. The same issue arises even for electrically thin layers that are homogeneous.

One way to treat a surface-relief grating with smooth corrugations is to planarize it using a carefully devised mapping. Two very different planarization approaches involve (i) transformative optics wherein the periodically corrugated interface is mapped into a flat interface by a change of spatial variables [30] and (ii) a series of perturbations [11]. The transformation-optics approach results in spatially dependent constitutive parameters, but opens the way to a Fourier-series-based solver (such as the RCWA) for the resulting equations since the interface has been flattened. This approach will not work directly for sawtooth or rectangular gratings, but does yield a popular numerical technique for grating problems [31, 32, 33, 34]. In the perturbative method of Nicholls *et al.* [11], the smooth corrugation is considered as the deformation of a flat interface via a Taylor series, and the effect of this deformation can be computed by solving a perturbative sequence of boundary-value problems by a Fourier technique. Both *s* and *p*-polarized incident waves have been considered and this approach is attractive because higher-order correctors can be incorporated.

Recently, Delourme *et al.* replaced an electrically thin annulus [35] and an electrically thin plate of finite extent [36, 37], both periodically nonhomogeneous by a circle and a finite-sized plane, respectively, on which they imposed transmission conditions that are different from the standard continuity conditions for the tangential components of the electric and magnetic field phasors on bi-medium interfaces. This planarization approach has been used by Özdemir *et al.* [38] for homogeneous and electrically thin regions of finite extent, and by Maurel *et al.* [39] for a periodic array of metallic bumps deposited on the planar surface of a dielectric material filling a half space.

Thus the planarization approach initiated by Delourme *et al.* [35, 36, 37] for regions of finite extent is applicable to electrically thin grating layers of infinite transverse extent, whether involving highly dissipative or weakly dissipative materials. When this (i.e., the third) planarization approach is used, there is no need of having extremely small elements in the FEM mesh for the grating layer. Moreover, the FEM mesh can be fixed for all possible geometric changes in the grating layer during an optimization process, which makes this technique suitable for determining optimal designs. Clearly, the third planarization approach differs from both the transformation-optics approach [30] and the perturbative approach [11].

In this paper, we adapt the third planarization approach to devise an asymptotic model so that the FEM can be implemented for shallow metallic gratings used as backreflectors in solar-cell structures [8, 9, 12]. Whether the incident plane wave is *s*- or *p*-polarized, the electrically thin grating layer is replaced by a planar interface across which certain transmission conditions hold and the Helmholtz equation is solved using the FEM. The grating interface can have corrugations that are rectangular, sawtooth, or of other shapes. This method is also applicable for an electrically thin homogeneous layer [38] since that layer can be conceptualized as a special case of a grating layer.

This paper is organized as follows. The boundary-value problem is set up and the asymptotic model is formulated in Sec. 2, when the grating geometry is invariant along the *y* axis, and the wave vector of the incident plane wave lies wholly in the *xz* plane. Numerical results to evaluate the performance of the

FEM incorporating the third planarization approach are presented and discussed in Sec. 3 for both  $s$ - and  $p$ -polarization states of the incident plane wave. The chief conclusions are summarized in Sec. 4. In the appendix we show that our approach can be generalized for application to a large-amplitude smooth grating perturbed by a thin grating with a smaller period [40].

An  $\exp(-i\omega t)$  dependence on time  $t$  is implicit, with  $\omega$  denoting the angular frequency and  $i = \sqrt{-1}$ . The free-space wavenumber, the free-space wavelength, and the intrinsic impedance of the free space are denoted by  $k_0 = \omega\sqrt{\varepsilon_0\mu_0}$ ,  $\lambda_0 = 2\pi/k_0$ , and  $\eta_0 = \sqrt{\mu_0/\varepsilon_0}$ , respectively, with  $\mu_0$  being the permeability and  $\varepsilon_0$  the permittivity of free space. Vectors are in boldface; Cartesian unit vectors are identified as  $\hat{\mathbf{u}}_x$ ,  $\hat{\mathbf{u}}_y$  and  $\hat{\mathbf{u}}_z$ ; and the position vector  $\mathbf{r} = x\hat{\mathbf{u}}_x + y\hat{\mathbf{u}}_y + z\hat{\mathbf{u}}_z$ .

## 2 Theory

### 2.1 Boundary-value problem

The solar-cell structure is assumed to occupy the region  $\Phi^\delta = \{\mathbf{r} \in \mathbb{R}^3 : |x| < \infty, |y| < \infty, -L_m - \delta/2 < z < \delta/2 + L_d\}$ . Within this region the relative permittivity  $\varepsilon_r(x, z) = \varepsilon_r(x \pm mL, z)$ ,  $m \in \mathbb{Z} = \{0, \pm 1, \pm 2, \dots\}$  is a function of  $x \in (-\infty, \infty)$  with period  $L$  and also varies with  $z \in (-L_m - \delta/2, \delta/2 + L_d)$  but not with  $y \in (-\infty, \infty)$ . The half spaces  $\{\mathbf{r} \in \mathbb{R}^3 : |x| < \infty, |y| < \infty, z < -L_m - \delta/2\}$  and  $\{\mathbf{r} \in \mathbb{R}^3 : |x| < \infty, |y| < \infty, z > \delta/2 + L_d\}$  are occupied by air; hence, the relative permittivity  $\varepsilon_r(x, z) \equiv 1$  in both these half spaces.

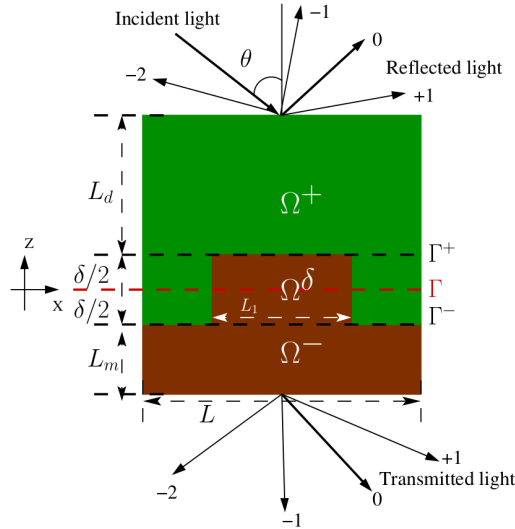


Figure 1: Unit cell  $\Omega = \Omega^+ \cup \Omega^\delta \cup \Omega^-$  of the solar-cell structure containing the grating layer of thickness  $\delta$ . The region  $\Omega^+$  lying above the plane  $\Gamma^+$  is occupied by an isotropic dielectric material (shaded green). The region  $\Omega^-$  lying below the plane  $\Gamma^-$  is occupied by an isotropic metal (shaded brown). Interposed between the planes  $\Gamma^-$  and  $\Gamma^+$ , the grating layer  $\Omega^\delta$  is magnified for clarity, but actually  $\delta \ll L$  for the planarization approach applied here.

The unit cell  $\Omega = \{\mathbf{r} \in \mathbb{R}^3 : 0 < x < L, |y| < \infty, -L_m - \delta/2 < z < \delta/2 + L_d\}$  of the solar-cell structure is shown schematically in Fig. 1, wherein we define the plane  $\Gamma = \{\mathbf{r} \in \mathbb{R}^3 : 0 < x < L, |y| < \infty, z = 0\}$ .

The domain  $\Omega$  is subdivided into the following three non-overlapping regions

$$\left. \begin{aligned} \Omega^- &= \left\{ \mathbf{r} \in \mathbb{R}^3 : 0 < x < L, |y| < \infty, \right. \\ &\quad \left. -L_m - \delta/2 < z < -\delta/2 \right\} \\ \Omega^\delta &= \left\{ \mathbf{r} \in \mathbb{R}^3 : 0 < x < L, |y| < \infty, \right. \\ &\quad \left. -\delta/2 < z < \delta/2 \right\} \\ \Omega^+ &= \left\{ \mathbf{r} \in \mathbb{R}^3 : 0 < x < L, |y| < \infty, \right. \\ &\quad \left. \delta/2 < z < \delta/2 + L_d \right\} \end{aligned} \right\} \quad (1)$$

separated by the non-intersecting planes

$$\left. \begin{aligned} \Gamma^- &= \left\{ \mathbf{r} \in \mathbb{R}^3 : (\mathbf{r} + \delta \hat{\mathbf{u}}_z/2) \in \Gamma \right\} \\ \Gamma^+ &= \left\{ \mathbf{r} \in \mathbb{R}^3 : (\mathbf{r} - \delta \hat{\mathbf{u}}_z/2) \in \Gamma \right\} \end{aligned} \right\}. \quad (2)$$

The grating layer  $\Omega^\delta$  is thus bounded by the planes  $\Gamma^-$  and  $\Gamma^+$ , with  $\min_x \{g(x)\} = -\delta/2$  and  $\max_x \{g(x)\} = \delta/2$ . Each of these three regions have different dielectric properties:  $\Omega^-$  is occupied by a homogeneous metal of relative permittivity  $\varepsilon_r^-$ ,  $\Omega_+$  is occupied by an isotropic dielectric material of relative permittivity  $\varepsilon_r^+$ , and  $\Omega^\delta$  is occupied by a periodically nonhomogeneous material with relative permittivity  $\varepsilon_r^\delta(x, z) = \varepsilon_r^\delta(x \pm L, z)$ .

The boundary  $z = \delta/2 + L_d$  of the solar-cell structure is illuminated by an obliquely incident plane wave whose electric field phasor is given by

$$\mathbf{E}_{\text{inc}}(\mathbf{r}) = [a_s \hat{\mathbf{u}}_y + a_p (\hat{\mathbf{u}}_x \cos \theta + \hat{\mathbf{u}}_z \sin \theta)] \exp \{ i k_0 [x \sin \theta - (z - \delta/2 - L_d) \cos \theta] \}, \quad z \geq \delta/2 + L_d, \quad (3)$$

where  $\theta$  is the angle of incidence with respect to the  $z$  axis,  $a_s$  is the amplitude of the  $s$ -polarized component, and  $a_p$  is the amplitude of the  $p$ -polarized component. The electric field phasors of the reflected and transmitted fields can be stated respectively as

$$\mathbf{E}_{\text{ref}}(\mathbf{r}) = \sum_{n \in \mathbb{Z}} \left( a_s r_s^{(n)} \hat{\mathbf{u}}_y + a_p r_p^{(n)} \mathbf{p}_n^+ \right) \exp \left\{ i \left[ \kappa^{(n)} x + \alpha^{(n)} (z - \delta/2 - L_d) \right] \right\}, \quad z > \delta/2 + L_d, \quad (4)$$

$$\mathbf{E}_{\text{tr}}(\mathbf{r}) = \sum_{n \in \mathbb{Z}} \left( a_s t_s^{(n)} \hat{\mathbf{u}}_y + a_p t_p^{(n)} \mathbf{p}_n^- \right) \exp \left\{ i \left[ \kappa^{(n)} x - \alpha^{(n)} (z + L_m + \delta/2) \right] \right\}, \quad z < -L_m - \delta/2, \quad (5)$$

where

$$\kappa^{(n)} = k_0 \sin \theta + 2\pi n/L, \quad (6)$$

$$\alpha^{(n)} = \begin{cases} +\sqrt{k_0^2 - (\kappa^{(n)})^2}, & k_0^2 \geq (\kappa^{(n)})^2 \\ +i\sqrt{(\kappa^{(n)})^2 - k_0^2}, & k_0^2 < (\kappa^{(n)})^2 \end{cases}, \quad (7)$$

and

$$\mathbf{p}_n^\pm = \mp \frac{\alpha^{(n)}}{k_0} \hat{\mathbf{u}}_x + \frac{\kappa^{(n)}}{k_0} \hat{\mathbf{u}}_z. \quad (8)$$

The reflection coefficients of order  $n \in \mathbb{Z}$  are denoted by  $r_s^{(n)}$  and  $r_p^{(n)}$ , and the corresponding transmission coefficients by  $t_s^{(n)}$  and  $t_p^{(n)}$ . For an  $s$ -polarized incident plane wave, the absorptance is defined as

$$A_s = 1 - \sum_{n \in \mathbb{Z}} \left[ (|r_s^{(n)}|^2 + |t_s^{(n)}|^2) \operatorname{Re}(\alpha^{(n)})/\alpha^{(0)} \right] \in [0, 1]; \quad (9)$$

for a  $p$ -polarized incident plane wave, the absorptance is given by

$$A_p = 1 - \sum_{n \in \mathbb{Z}} \left[ (|r_p^{(n)}|^2 + |t_p^{(n)}|^2) \operatorname{Re}(\alpha^{(n)})/\alpha^{(0)} \right] \in [0, 1]. \quad (10)$$

Both quantities are functions of  $\lambda_0$  and  $\theta$ .

## 2.2 Scalar equations and boundary conditions

The time-harmonic form of the Maxwell curl equations is given by

$$\left. \begin{aligned} \nabla \times \mathbf{E}(\mathbf{r}) &= i\omega\mu_0\mathbf{H}(\mathbf{r}), \\ \nabla \times \mathbf{H}(\mathbf{r}) &= -i\omega\varepsilon_0\varepsilon_r(x,z)\mathbf{E}(\mathbf{r}), \end{aligned} \right\}, \quad \mathbf{r} \in \Omega. \quad (11)$$

After decoupling the  $s$ - and  $p$ -polarization states since the fields do not depend on  $y$ , Eqs. (11) reduce to the Helmholtz equation

$$\nabla \cdot [B(x,z)\nabla u(x,z)] + k_0^2 b(x,z)u(x,z) = 0, \quad \mathbf{r} \in \Omega, \quad (12)$$

where

$$u(x,z) = E_y(x,z), \quad B(x,z) = 1, \quad b(x,z) = \varepsilon_r(x,z), \quad (13)$$

for the  $s$  polarization state, and

$$u(x,z) = -\eta_0 H_y(x,z), \quad B(x,z) = \frac{1}{\varepsilon_r(x,z)}, \quad b(x,z) = 1, \quad (14)$$

for the  $p$  polarization state.

The solution  $u(x,z)$  is denoted by  $u^+(x,z)$  and  $u^-(x,z)$ , respectively, for  $z > \delta/2 + L_d$  and  $z < -L_m - \delta/2$ . Equations (3)–(5) lead to the expansions

$$u^+(x,z) = a_q \exp \left\{ i \left[ \kappa^{(0)} x - \alpha^{(0)} (z - \delta/2 - L_d) \right] \right\} + a_q \sum_{n \in \mathbb{Z}} r_q^{(n)} \exp \left\{ i \left[ \kappa^{(n)} x + \alpha^{(n)} (z - \delta/2 - L_d) \right] \right\}, \quad (15)$$

$$z > \delta/2 + L_d,$$

$$u^-(x,z) = a_q \sum_{n \in \mathbb{Z}} t_q^{(n)} \exp \left\{ i \left[ \kappa^{(n)} x - \alpha^{(n)} (z + L_m + \delta/2) \right] \right\}, \quad z < -L_m - \delta/2, \quad (16)$$

where  $q \in \{p, s\}$ .

The functions  $u(x,z)$  and  $u^-(x,z)$  must be appropriately matched using standard continuity conditions on the plane  $z = -L_m - \delta/2$ , and the functions  $u(x,z)$  and  $u^+(x,z)$  match in the same way on the plane  $z = \delta/2 + L_d$ . Hence, with  $\rho > 0$ , we have to enforce the conditions

$$\left. \begin{aligned} u^-(x,z)|_{z=-L_m-\delta/2-\rho} &= u(x,z)|_{z=-L_m-\delta/2+\rho} \\ \frac{\partial u^-(x,z)}{\partial z}|_{z=-L_m-\delta/2-\rho} &= B(x,z) \frac{\partial u(x,z)}{\partial z}|_{z=-L_m-\delta/2+\rho} \\ u^+(x,z)|_{z=\delta/2+L_d+\rho} &= u(x,z)|_{z=\delta/2+L_d-\rho} \\ \frac{\partial u^+(x,z)}{\partial z}|_{z=\delta/2+L_d+\rho} &= B(x,z) \frac{\partial u(x,z)}{\partial z}|_{z=\delta/2+L_d-\rho} \end{aligned} \right\}, \quad (17)$$

$$x \in [0, L],$$

in the limit  $\rho \rightarrow 0$ . In addition,  $u(x,z)$  satisfies the quasi-periodicity conditions

$$\left. \begin{aligned} u(x,z)|_{x=L} &= \exp(i\kappa^{(0)}L)u(x,z)|_{x=0} \\ \hat{\mathbf{u}}_\Gamma \cdot \nabla u(x,z)|_{x=L} &= \exp(i\kappa^{(0)}L)\hat{\mathbf{u}}_\Gamma \cdot \nabla u(x,z)|_{x=0} \end{aligned} \right\}, \quad (18)$$

$$z \in (-L_m - \delta/2, \delta/2 + L_d),$$

where the unit vector  $\hat{\mathbf{u}}_\Gamma = \hat{\mathbf{u}}_z$  is normal to the plane  $\Gamma$ .

## 2.3 Asymptotic model

Equations (12)–(18) constitute the *full model* which we approximate by an *asymptotic model* (valid in the limit when  $\delta \rightarrow 0$ ) where  $\Omega^\delta$  is replaced by the plane  $\Gamma$ . In the asymptotic model, the approximation of the fields must satisfy certain *approximate transmission conditions* (ATCs) across  $\Gamma$ .

There is no unique way to prescribe the ATCs. For instance, Maurel *et al.* [39] used an approach similar to the one analyzed by Delourme *et al.* [35, 36, 37] where each term of the power series in the asymptotic expansions is written as a Taylor series around  $z = 0$  (i.e., the plane  $\Gamma$ ). Then, both fields are matched in a suitable overlapping region. Undertaking this approach, Maurel *et al.* derived ATCs correct to order  $\delta$ , with the coefficients (usually called *interface parameters*) in the ATCs determined by solving the partial differential equations satisfied by the fields in the asymptotic expansions. The solution of these equations might be costly, depending on the corrugation shape. However, in particular cases such as the rectangular corrugations considered by Maurel *et al.* [39], the interface parameters can be approximately determined.

Özdemir *et al.* [38] proposed another way to define the ATCs, provided the thin layer  $\Omega^\delta$  is occupied by a homogeneous material, i.e., when  $\varepsilon_r^\delta(x, z)$  depends on neither  $x$  nor  $z$ . In this work we generalize their approach to our setting wherein  $\varepsilon_r^\delta(x, z) = \varepsilon_r^\delta(x \pm L, z)$  as follows.

Although  $u(x, z)$  is represented by Eqs. (15) and (16), respectively, for  $z > \delta/2 + L_d$  and  $z < -L_m - \delta/2$ , respectively, we need to represent  $u(x, z)$  in  $\Omega$  as well. This is done by adopting separate representations in the three parts of  $\Omega$ ; thus,

$$u(x, z) = \begin{cases} u_\delta^-(x, z) \\ u^\delta(x, z) \\ u_\delta^+(x, z) \end{cases}, \quad \mathbf{r} \in \begin{cases} \Omega^- \\ \Omega^\delta \\ \Omega^+ \end{cases}. \quad (19)$$

Concurrently, we define

$$B(x, z) = \begin{cases} B^-(x, z) \\ B^\delta(x, z) \\ B^+(x, z) \end{cases}, \quad b(x, z) = \begin{cases} b^-(x, z) \\ b^\delta(x, z) \\ b^+(x, z) \end{cases}, \quad \mathbf{r} \in \begin{cases} \Omega^- \\ \Omega^\delta \\ \Omega^+ \end{cases}. \quad (20)$$

Equation (12) then devolves into the three partial differential equations

$$\nabla \cdot [B^\pm(x, z) \nabla u_\delta^\pm(x, z)] + k_0^2 b^\pm(x, z) u_\delta^\pm(x, z) = 0, \quad \mathbf{r} \in \Omega^\pm, \quad (21)$$

and

$$\nabla \cdot [B^\delta(x, z) \nabla u^\delta(x, z)] + k_0^2 b^\delta(x, z) u^\delta(x, z) = 0, \quad \mathbf{r} \in \Omega^\delta. \quad (22)$$

With  $\rho > 0$ , Eqs. (21) and (22) must be solved subject to the continuity conditions

$$\left. \begin{aligned} u_\delta^-(x, z)|_{z=-\delta/2-\rho} &= u^\delta(x, z)|_{z=-\delta/2+\rho} \\ B^-(x, z) \frac{\partial u_\delta^-(x, z)}{\partial z} \Big|_{z=-\delta/2-\rho} &= B^\delta(x, z) \frac{\partial u^\delta(x, z)}{\partial z} \Big|_{z=-\delta/2+\rho} \\ u_\delta^+(x, z)|_{z=\delta/2+\rho} &= u^\delta(x, z)|_{z=\delta/2-\rho} \\ B^+(x, z) \frac{\partial u_\delta^+(x, z)}{\partial z} \Big|_{z=\delta/2+\rho} &= B^\delta(x, z) \frac{\partial u^\delta(x, z)}{\partial z} \Big|_{z=\delta/2-\rho} \end{aligned} \right\}, \quad (23)$$

$$x \in [0, L],$$

in the limit  $\rho \rightarrow 0$ .

In our asymptotic model, the domain  $\Omega^\delta$  is replaced by the plane  $\Gamma$ . Hence, the functions  $B^\delta(x, z)$  and  $b^\delta(x, z)$  must be approximated by functions that can only depend on  $x$ . Therefore, we average the relative permittivity over  $z \in (-\delta/2, \delta/2)$  as

$$\overline{\varepsilon_r(x)} = \frac{1}{\delta} \int_{-\delta/2}^{\delta/2} \varepsilon_r(x, z) dz \quad (24)$$

and set

$$\overline{B^\delta(x)} = \begin{cases} 1 \\ \left( \overline{\varepsilon_r(x)} \right)^{-1} \end{cases}, \quad \overline{b^\delta(x)} = \begin{cases} \overline{\varepsilon_r(x)} \\ 1 \end{cases}, \quad \text{pol. state} = \begin{cases} s \\ p \end{cases}. \quad (25)$$

Next, we scale the solution in  $\Omega^\delta$  with respect to the thickness of the grating layer by changing the variable  $z$  to  $\xi = z/\delta$ . This scaling defines the domain

$$\begin{aligned} \tilde{\Omega}^\delta = \{ \tilde{\mathbf{r}} = x\hat{\mathbf{u}}_x + y\hat{\mathbf{u}}_y + \xi\hat{\mathbf{u}}_z \in \mathbb{R}^3 : 0 < x < L, |y| < \infty, \\ -1/2 < \xi < 1/2 \} \end{aligned} \quad (26)$$

and allows us to remove the dependences of various quantities on the small parameter  $\delta$ . After defining the scaled function  $\tilde{u}^\delta(x, \xi) = u^\delta(x, \delta\xi)$ , and using the chain rule as well as the  $z$ -averaged quantities introduced in Eq. (25), (22) can be rewritten approximately as

$$\frac{\partial}{\partial x} \left( \overline{B^\delta(x)} \frac{\partial \tilde{u}^\delta(x, \xi)}{\partial x} \right) + \frac{1}{\delta^2} \frac{\partial}{\partial \xi} \left( \overline{B^\delta(x)} \frac{\partial \tilde{u}^\delta(x, \xi)}{\partial \xi} \right) + k_0^2 \overline{b^\delta(x)} \tilde{u}^\delta(x, \xi) = 0, \quad \tilde{\mathbf{r}} \in \tilde{\Omega}^\delta. \quad (27)$$

Let us now assume that  $\tilde{u}^\delta(x, \xi)$  can be written as the power series

$$\tilde{u}^\delta(x, \xi) = \sum_{j=0}^{\infty} \delta^j \tilde{u}_j^\delta \left( x, \frac{z}{\delta} \right). \quad (28)$$

Then, after inserting the asymptotic expansion on the right side of (27) into (27), equating the terms having the same powers of  $\delta$ , and using the convention that  $\tilde{u}_\ell^\delta = 0$  for  $\ell < 0$ , we obtain

$$\frac{\partial}{\partial x} \left( \overline{B^\delta(x)} \frac{\partial \tilde{u}_{j-2}^\delta(x, \xi)}{\partial x} \right) + \frac{\partial}{\partial \xi} \left( \overline{B^\delta(x)} \frac{\partial \tilde{u}_j^\delta(x, \xi)}{\partial \xi} \right) + k_0^2 \overline{b^\delta(x)} \tilde{u}_{j-2}^\delta(x, \xi) = 0, \quad \tilde{\mathbf{r}} \in \tilde{\Omega}^\delta, \quad j \in \{0, 1, \dots\}. \quad (29)$$

Let us also assume that the solution can be represented in the regions  $\Omega^\pm$  as a power series with respect to  $\delta$ ; i.e.,

$$u_\delta^\pm(x, z) = \sum_{j=0}^{\infty} \delta^j \varphi_j^\pm(x, z). \quad (30)$$

As is usual in asymptotic models of this type, the functions  $\varphi_j^\pm$  are assumed to be at least once differentiable with respect to  $z$ . In addition, due to the quasi-periodicity conditions in Eqs. (18), it is natural to assume that  $\varphi_j^\pm$  are quasi-periodic with respect to  $x$ .

After replacing  $B^\delta(x, z)$  by its averaged value  $\overline{B^\delta(x)}$  and  $u^\delta(x, z)$  by  $\tilde{u}^\delta(x, \xi)$  in Eqs. (23), those continuity conditions simplify to

$$\left. \begin{aligned} u_\delta^- (x, z) \Big|_{z=-\frac{\delta}{2}-\rho} &= \tilde{u}^\delta(x, \xi) \Big|_{\xi=-\frac{1}{2}+\rho} \\ \left( B^- (x, z) \frac{\partial u_\delta^- (x, z)}{\partial z} \right) \Big|_{z=-\frac{\delta}{2}-\rho} &= \frac{1}{\delta} \left( \overline{B^\delta(x)} \frac{\partial \tilde{u}^\delta(x, \xi)}{\partial \xi} \right) \Big|_{\xi=-\frac{1}{2}+\rho} \\ u_\delta^+ (x, z) \Big|_{z=\frac{\delta}{2}+\rho} &= \tilde{u}^\delta(x, \xi) \Big|_{\xi=\frac{1}{2}-\rho} \\ \left( B^+ (x, z) \frac{\partial u_\delta^+ (x, z)}{\partial z} \right) \Big|_{z=\frac{\delta}{2}+\rho} &= \frac{1}{\delta} \left( \overline{B^\delta(x)} \frac{\partial \tilde{u}^\delta(x, \xi)}{\partial \xi} \right) \Big|_{\xi=\frac{1}{2}-\rho} \end{aligned} \right\}, \quad x \in [0, L] \quad (31)$$

in the limit  $\rho \rightarrow 0$ . On using Eqs. (28) and (30) in Eqs. (31) and after equating the terms with the same powers of  $\delta$ , we finally obtain the continuity conditions

$$\left. \begin{aligned} \phi_j^- (x, z) \Big|_{z=-\frac{\delta}{2}-\rho} &= \tilde{u}_j^\delta(x, \xi) \Big|_{\xi=-\frac{1}{2}+\rho} \\ \left( B^- (x, z) \frac{\partial \phi_{j-1}^- (x, z)}{\partial z} \right) \Big|_{z=-\frac{\delta}{2}-\rho} &= \left( \overline{B^\delta(x)} \frac{\partial \tilde{u}_j^\delta(x, \xi)}{\partial \xi} \right) \Big|_{\xi=-\frac{1}{2}+\rho} \\ \phi_j^+ (x, z) \Big|_{z=\frac{\delta}{2}+\rho} &= \tilde{u}_j^\delta(x, \xi) \Big|_{\xi=\frac{1}{2}-\rho} \\ \left( B^+ (x, z) \frac{\partial \phi_{j-1}^+ (x, z)}{\partial z} \right) \Big|_{z=\frac{\delta}{2}+\rho} &= \left( \overline{B^\delta(x)} \frac{\partial \tilde{u}_j^\delta(x, \xi)}{\partial \xi} \right) \Big|_{\xi=\frac{1}{2}+\rho} \end{aligned} \right\},$$

$$x \in [0, L], \quad j \in \{0, 1, \dots\}, \quad (32)$$

in the limit  $\rho \rightarrow 0$ .

Let

$$v(x, z) = \begin{cases} v^-(x, z) \\ v^+(x, z) \end{cases}, \quad \mathbf{r} \in \begin{cases} \Omega^- \\ \Omega^+ \end{cases} \quad (33)$$

be any function defined in  $\Omega^- \cup \Omega^+$ . We denote by  $[v]$  and  $\langle v \rangle$ , respectively, the *jump* and *mean* values of  $v$  defined as

$$\left. \begin{aligned} [v](x) &= v^+(x, z)|_{z=\frac{\delta}{2}+\rho} - v^-(x, z)|_{z=-\frac{\delta}{2}-\rho} \\ \langle v \rangle(x) &= \frac{1}{2} \left( v^+(x, z)|_{z=\frac{\delta}{2}+\rho} + v^-(x, z)|_{z=-\frac{\delta}{2}-\rho} \right) \\ x &\in [0, L], \end{aligned} \right\} \quad (34)$$

in the limit  $\rho \rightarrow 0$ .

Using this notation along with Barrow's rule in Eqs. (32), we obtain the relations

$$\left. \begin{aligned} \overline{B^\delta(x)} \frac{\partial \tilde{u}_j^\delta}{\partial \xi}(x, \xi) &= \left\langle B \frac{\partial \varphi_{j-1}}{\partial z} \right\rangle(x) + \frac{1}{2} \left[ \int_{-\frac{1}{2}}^\xi \frac{\partial}{\partial \tau} \left( \overline{B^\delta(x)} \frac{\partial \tilde{u}_j^\delta(x, \tau)}{\partial \tau} \right) d\tau - \int_\xi^{\frac{1}{2}} \frac{\partial}{\partial \tau} \left( \overline{B^\delta(x)} \frac{\partial \tilde{u}_j^\delta(x, \tau)}{\partial \tau} \right) d\tau \right] \\ \tilde{u}_j^\delta(x, \xi) &= \langle \varphi_j \rangle(x) + \frac{1}{2} \left( \int_{-\frac{1}{2}}^\xi \frac{\partial \tilde{u}_j^\delta}{\partial \tau}(x, \tau) d\tau - \int_\xi^{\frac{1}{2}} \frac{\partial \tilde{u}_j^\delta}{\partial \tau}(x, \tau) d\tau \right) \\ \left[ B \frac{\partial \varphi_j}{\partial z} \right](x) &= \int_{-\frac{1}{2}}^{\frac{1}{2}} \frac{\partial}{\partial \tau} \left( \overline{B^\delta(x)} \frac{\partial \tilde{u}_{j+1}^\delta(x, \tau)}{\partial \tau} \right) d\tau \\ [\varphi_j](x) &= \int_{-\frac{1}{2}}^{\frac{1}{2}} \frac{\partial \tilde{u}_j^\delta}{\partial \tau}(x, \tau) d\tau \\ x &\in [0, L], \quad \xi \in [-1/2, 1/2]. \end{aligned} \right\} \quad (35)$$

Using these relations, we can write  $\left[ B \frac{\partial \varphi_j}{\partial z} \right](x)$  and  $[\varphi_j](x)$  in terms of  $\left\langle B \frac{\partial \varphi_{j-1}}{\partial z} \right\rangle(x)$  and  $\langle \varphi_{j-1} \rangle(x)$ . In particular, for  $j \in \{0, 1, 2\}$ , we get

$$\left. \begin{aligned} [\varphi_0](x) &= 0 \\ \left[ B \frac{\partial \varphi_0}{\partial z} \right](x) &= 0 \\ [\varphi_1](x) &= \left( \overline{B^\delta(x)} \right)^{-1} \left\langle B \frac{\partial \varphi_0}{\partial z} \right\rangle(x) \\ \left[ B \frac{\partial \varphi_1}{\partial z} \right](x) &= - \left( \frac{\partial}{\partial x} \left( \overline{B^\delta(x)} \frac{\partial}{\partial x} \right) + k_0^2 \overline{b^\delta(x)} \right) \langle \varphi_0 \rangle(x) \\ [\varphi_2](x) &= \left( \overline{B^\delta(x)} \right)^{-1} \left\langle B \frac{\partial \varphi_1}{\partial z} \right\rangle(x) \\ \left[ B \frac{\partial \varphi_2}{\partial z} \right](x) &= - \left( \frac{\partial}{\partial x} \left( \overline{B^\delta(x)} \frac{\partial}{\partial x} \right) + k_0^2 \overline{b^\delta} \right) \langle \varphi_1 \rangle(x) \end{aligned} \right\}, \quad (36)$$

$$x \in [0, L].$$

Let us now restrict the summation on the right side of Eq. (30) to  $j \in \{0, 1, 2\}$  so that

$$u_\delta^\pm(x, z) \approx u_{\delta,2}^\pm(x, z) = \varphi_0^\pm(x, z) + \delta \varphi_1^\pm(x, z) + \delta^2 \varphi_2^\pm(x, z). \quad (37)$$

Equations (36) then yield

$$\left. \begin{aligned} [u_{\delta,2}](x) &= \delta \left( \overline{B^\delta(x)} \right)^{-1} \left\langle B \frac{\partial u_{\delta,2}}{\partial z} \right\rangle(x) - \delta^3 \left( \overline{B^\delta(x)} \right)^{-1} \left\langle B \frac{\partial \varphi_2}{\partial z} \right\rangle(x) \\ \left[ B \frac{\partial u_{\delta,2}}{\partial z} \right](x) &= -\delta \left( \frac{\partial}{\partial x} \left( \overline{B^\delta(x)} \frac{\partial}{\partial x} \right) + k_0^2 \overline{b^\delta(x)} \right) \langle u_{\delta,2} \rangle(x) + \delta^3 \left( \frac{\partial}{\partial x} \left( \overline{B^\delta(x)} \frac{\partial}{\partial x} \right) + k_0^2 \overline{b^\delta(x)} \right) \langle \varphi_2 \rangle(x). \end{aligned} \right\},$$

$$x \in [0, L]. \quad (38)$$

Neglecting terms of order  $\delta^3$ , we finally obtain the following transmission conditions for  $u_{\delta,2}^{\pm}(x, z)$ :

$$\left. \begin{aligned} [u_{\delta,2}] (x) &= \delta \left( \overline{B^{\delta}(x)} \right)^{-1} \left\langle B \frac{\partial u_{\delta,2}}{\partial z} \right\rangle (x) \\ \left[ B \frac{\partial u_{\delta,2}}{\partial z} \right] (x) &= -\delta \left( \frac{\partial}{\partial x} \left( \overline{B^{\delta}(x)} \frac{\partial}{\partial x} \right) + k_0^2 \overline{b^{\delta}(x)} \right) \langle u_{\delta,2} \rangle (x) \end{aligned} \right\},$$

$$x \in [0, L]. \quad (39a)$$

The above conditions are called ATCs because they correspond to approximations up to second order of the transmission conditions satisfied by  $u_{\delta,2}^{\pm}$ . The interface parameters are  $\overline{B^{\delta}(x)}$  and  $\overline{b^{\delta}(x)}$ . In addition, according to (21),  $u_{\delta,2}^{\pm}$  satisfy the partial differential equations

$$\nabla \cdot \left[ B^{\pm} \nabla u_{\delta,2}^{\pm}(x, z) \right] + k_0^2 b^{\pm}(x, z) u_{\delta,2}^{\pm}(x, z) = 0, \quad \mathbf{r} \in \Omega^{\pm}, \quad (39b)$$

together with the bottom and top transmission conditions in Eqs. (17) and the quasi-periodic boundary conditions in Eqs. (18). After solving Eqs. (39) for  $u_{\delta,2}^{\pm}(x, z)$ , we can approximately determine  $u_{\delta}^{\pm}(x, z)$  in  $\Omega^{\pm}$ .

In the asymptotic model thus,  $\delta$  has been removed from the geometry (i.e., the region  $\Omega^{\delta}$  has been flattened into the plane  $\Gamma$ ) and is now contained in the expansion coefficients of the solution in  $\Omega^{\pm}$ . Since terms of order  $\delta^3$  were neglected, the best possible truncation error is likely to be of order  $\delta^3$ . As we show in Sec. 3, this indeed occurs for grating layers that are homogeneous, but a slower convergence (better than second order) is observed for nonhomogeneous grating layers possibly due to the replacement of  $\epsilon_r(x, z)$  by  $\overline{\epsilon_r(x)}$  in the region  $\Omega^{\delta}$  and to the effect of the corrugation in the FEM solution. This issue would require further investigation and will be addressed elsewhere, since the goal of this paper is to describe and numerically analyze the behavior of the method. The convergence of the asymptotic model can be studied following the procedure of Delourme *et al.* [35, 36].

### 3 Numerical results

Let us now demonstrate numerically the convergence properties of the asymptotic model. We chose to solve Eqs. (39) using standard Lagrange FEM with third-degree polynomials, subject to the transmission conditions in Eqs. (17) across the planes  $z = \delta/2 + L_d$  and  $z = -L_m - \delta/2$ , following the procedure described, for instance, by Solano *et al.* [24].

Results are presented for three examples. In the first two examples we focus on the convergence of the asymptotic model at the fixed wavelength  $\lambda_0 = 450$  nm. In the third example we examine the performance of the asymptotic model in the range  $\lambda_0 \in [400, 1000]$  nm. For all three examples, we fixed  $L = 400$  nm,  $L_d = 125$  nm,  $L_m = 50$  nm. We also fixed  $\theta = 0$  deg, as most solar cells are illuminated normally to maximize photonic absorption. The material with the relative permittivity  $\epsilon_r^+$  was taken to be evaporated silver whereas that with the relative permittivity  $\epsilon_r^-$  was amorphous silicon nitride, both  $\epsilon_r^+$  and  $\epsilon_r^-$  being frequency dependent [41]. The chosen value of  $L_m$  exceeds the skin depth of silver, ensuring that transmission into the half space  $z < L_m - \delta/2$  is minuscule at best. We chose values of  $\delta$  between 0.3906 and 12 nm. Then, the maximum value of  $\delta$  is 6.67% of the total height  $L_m + L_d + \delta$  of the solar-cell structure, and the minimum value of  $\delta$  is 0.22% of the total height.

Finally, the series on the right sides of Eqs. (15) and (16) have to be truncated so that  $|n| \leq M_t$ . This truncation error is the same for both the full and asymptotic models. Since our goal with the first two examples was to analyze convergence with respect to  $\delta$ , the value of  $M_t$  will have no influence. Hence, we fixed  $M_t = 3$  in order to speed up the calculations. For the third example, we took  $M_t = 20$  as

in a previous paper [24] in order to diminish the influence of this truncation error when examining the absorbance spectra.

The domain  $\Omega$  was discretized into  $N_e$  triangular elements, with the length of the largest edge denoted by  $h$ . Let  $u_{\delta,2}^{q,h}(x,z)$  and  $A_q^h$  denote the values of  $u_{\delta,2}^q(x,z)$  and  $A_q$ , respectively, delivered by our asymptotic model for a specific choice of  $h$  when the polarization state of the incident plane wave is either  $q = s$  or  $q = p$ . The errors in our calculations are of two types: (i) those due to the use of the FEM and (ii) those due to the asymptotic model.

### 3.1 Example 1: Planar Backreflector

Let us begin by choosing the backreflector as planar and the material occupying  $\Omega^\delta$  to have the uniform relative permittivity  $\varepsilon_r^\delta(x,z) \equiv -1.0976 + 0.3325i$ . For this problem, the solution  $u^q(x,z)$ ,  $q \in \{s,p\}$ , of (12) can be exactly determined everywhere using a textbook approach [42]. For each polarization state, we computed the relative errors

$$\left. \begin{aligned} e_{u_q} &= \frac{\left( \int_{\Omega^+ \cup \Omega^-} |u^q - u_{\delta,2}^{q,h}|^2 dx dz \right)^{1/2}}{\left( \int_{\Omega^+ \cup \Omega^-} |u^q|^2 dx dz \right)^{1/2}} \\ e_{A_q} &= \frac{|A_q - A_q^h|}{|A_q|} \end{aligned} \right\}, \quad q \in \{s,p\}. \quad (40)$$

Since  $e_{u_s}$  and  $e_{u_p}$  evinced similar trends with respect to changes in  $h$  and  $\delta$ , and so did  $A_s$  and  $A_p$ , let us confine our attention to the  $p$ -polarization state in the remainder of Sec. 33.1.

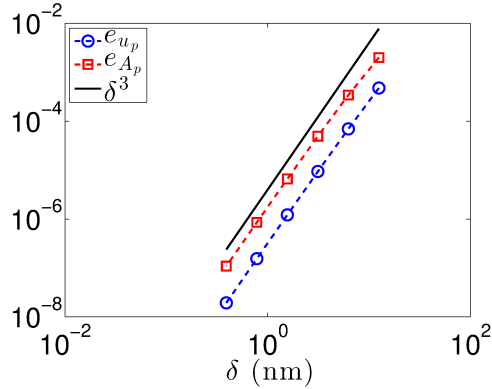


Figure 2: Calculated values of the relative errors  $e_{u_p}$  (identified by blue  $\circ$ ) and  $e_{A_p}$  (red  $\square$ ) versus  $\delta$  when  $h = 2.21$  nm for the planar metallic backreflector of Sec. 33.1. Dashed lines guide the reader's eyes. Solid black line indicates the  $\delta^3$  dependence.

First, in order to evaluate the performance of the asymptotic model with respect to the parameter  $\delta$ ,  $e_{u_p}$  and  $e_{A_p}$  are plotted versus  $\delta$  in Fig. 2, for the smallest value of  $h$  ( $= 2.21$  nm) in our study. Both  $e_{u_p}$  and  $e_{A_p}$  are of order  $\delta^3$ , as expected.

Next, in order to validate our FEM solver, in Fig. 3 we display  $e_{u_p}$  versus  $h$  for  $\delta = 0.3906$  nm. Standard FEM theory [43] predicts that the rate of convergence of  $e_{u_p}$  must be of order  $h^4$ . In Fig. 3 we observe exactly this trend, except for the smallest value of  $h$  where it seems that the asymptotic-model error dominates the FEM error and that is why the  $h^4$  dependence can not be observed for the smaller values of  $h$ .

Table 1: Relative error  $e_{u_p}$  versus  $\delta$  (nm) and  $h$  (nm) for Example 1 (Sec. 33.1). The number  $N_e$  of triangular elements is shown in parentheses for each of the three values of  $h$  in the table.

$h \setminus (N_e)$ $\delta$ (nm)	35.36 (224)	17.68 (896)	8.84 (3584)
12.5	$4.8053 \times 10^{-4}$	$4.7755 \times 10^{-4}$	$4.7750 \times 10^{-4}$
6.25	$9.6565 \times 10^{-5}$	$6.9828 \times 10^{-5}$	$6.9664 \times 10^{-5}$
3.125	$7.0314 \times 10^{-5}$	$1.0299 \times 10^{-5}$	$9.3360 \times 10^{-6}$
1.5625	$7.0992 \times 10^{-5}$	$4.4827 \times 10^{-6}$	$1.1926 \times 10^{-6}$
0.7812	$7.1811 \times 10^{-5}$	$4.3592 \times 10^{-6}$	$2.9804 \times 10^{-7}$
0.3906	$7.2338 \times 10^{-5}$	$4.3853 \times 10^{-6}$	$2.8574 \times 10^{-7}$

In Table 1 we display values of the relative error  $e_{u_p}$  while varying  $\delta$  (from top to bottom) and  $h$  (from left to right). All values of  $e_{u_p}$  are smaller than 0.05%. In the first row, we observe that the asymptotic-model error dominates the FEM error for  $\delta = 12.5$  nm, since  $e_{u_p}$  does not significantly decrease as  $h$  decreases. Similar conclusions were found to hold for  $\delta \in \{6.25, 3.125, 1.5625\}$  nm, i.e., the asymptotic-model error starts to dominate the FEM error when  $h < 17.68$  nm. On the other hand, when  $\delta$  is small, for example 0.3906 nm, the FEM error dominates the asymptotic-model error. In fact,  $e_{u_p}$  decreases 16 times when  $h$  is halved, i.e., the rate of convergence is of order  $h^4$  as predicted by the standard FEM theory ([43]). The trends evident in Table 1 for  $e_{u_p}$  are mirrored by those in Table 2 for  $e_{A_p}$ .

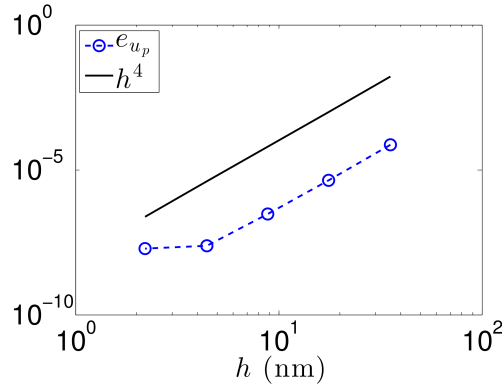


Figure 3: Calculated values (identified by blue  $\circ$ ) of the relative error  $e_{u_p}$  versus  $h$  when  $\delta = 0.3906$  nm for the planar metallic backreflector of Sec. 33.1. The dashed blue line guides the reader's eyes. The solid black line indicates the  $h^4$  dependence.

### 3.2 Example 2: Periodic Backreflector with Rectangular Corrugations

Next, we consider the backreflector to have rectangular corrugations of height  $\delta$  and width  $L_1 = \zeta L$ , as shown in Fig. 1. In the unit cell  $\Omega$ , the grating profile is described by the function

$$g(x) = \begin{cases} -\delta/2, & 0 \leq x < (1 - \zeta)L/2, \\ \delta/2, & (1 - \zeta)L/2 < x < (1 + \zeta)L/2, \\ -\delta/2, & (1 + \zeta)L/2 < x \leq L, \end{cases} \quad (41)$$

Table 2: Same as Table 1 but values of the relative error  $e_{A_p}$  are shown.

$h$ ( $N_e$ ) $\delta$ (nm)	35.36 (224)	17.68 (896)	8.84 (3584)
12.5	$2.0134 \times 10^{-3}$	$2.0090 \times 10^{-3}$	$2.0090 \times 10^{-3}$
6.25	$3.4851 \times 10^{-4}$	$3.4305 \times 10^{-4}$	$3.4307 \times 10^{-4}$
3.125	$5.5617 \times 10^{-5}$	$4.9543 \times 10^{-5}$	$4.9574 \times 10^{-5}$
1.5625	$1.3120 \times 10^{-5}$	$7.5367 \times 10^{-6}$	$6.8810 \times 10^{-6}$
0.7812	$6.7215 \times 10^{-6}$	$9.6876 \times 10^{-7}$	$2.2527 \times 10^{-7}$
0.3906	$6.7553 \times 10^{-6}$	$1.0040 \times 10^{-6}$	$2.6115 \times 10^{-7}$

with

$$\varepsilon_r^\delta(\mathbf{r}) = \begin{cases} \varepsilon_r^+ & z > g(x) \\ \varepsilon_r^- & z < g(x) \end{cases}, \quad \mathbf{r} \in \Omega^\delta. \quad (42)$$

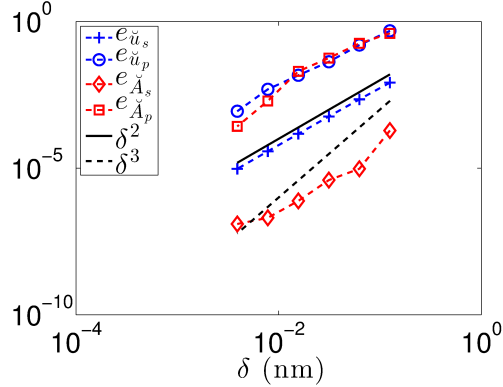


Figure 4: Calculated values of the relative errors  $e_{\check{u}_s}$  (identified by blue +),  $e_{\check{u}_p}$  (blue o),  $e_{\check{A}_s}$  (red  $\diamond$ ) and  $e_{\check{A}_p}$  (red  $\square$ ) versus  $\delta$  when  $h = 8.84$  nm for the metallic backreflector with rectangular corrugations described in Sec. 33.2. Dashed blue or red lines guide the reader's eyes. Solid-black and dashed-black lines indicate the  $\delta^2$  and  $\delta^3$  dependences, respectively.

As an exact solution  $u$  cannot be found for the chosen backreflector, we designated by  $\check{u}(x, z)$  the FEM solution obtained with the smallest value of  $h$  ( $= 2.21$  nm) in our study, and by  $\check{A}$  the corresponding absorptance. Using these results as the *reference solution*, we determined for  $\zeta = 0.5$  the relative errors

$$\left. \begin{aligned} e_{\check{u}_q} &= \frac{\left( \int_{\Omega^+ \cup \Omega^-} |\check{u}^q - u_{\delta,2}^{q,h}|^2 dx dz \right)^{1/2}}{\left( \int_{\Omega^+ \cup \Omega^-} |\check{u}^q|^2 dx dz \right)^{1/2}} \\ e_{\check{A}_q} &= \frac{|\check{A}_q - A_q^h|}{|\check{A}_q|} \end{aligned} \right\}, \quad q \in \{s, p\}, \quad (43)$$

as functions of  $\delta$  and  $h$ . This FEM-*reference* solution has been validated by comparing it with an RCWA solution. In fact, we have observed that the FEM-*reference* and RCWA solutions agree within 3% in absorptances and within 5% in the fields.

Table 3: Relative error  $e_{\check{u}_s}$  versus  $\delta$  (nm) and  $h$  (nm) for Example 2 (Sec. 33.2). The number  $N_e$  of triangular elements is shown in parentheses for each of the three values of  $h$  in the table.

$h$ ( $N_e$ ) $\delta$ (nm)	35.36 (224)	17.68 (896)	8.84 (3584)
12.5	$8.1484 \times 10^{-3}$	$8.1583 \times 10^{-3}$	$8.1610 \times 10^{-3}$
6.25	$2.2067 \times 10^{-3}$	$2.2049 \times 10^{-3}$	$2.2050 \times 10^{-3}$
3.125	$5.8389 \times 10^{-4}$	$5.7720 \times 10^{-4}$	$5.7700 \times 10^{-4}$
1.5625	$1.6766 \times 10^{-4}$	$1.4817 \times 10^{-4}$	$1.4790 \times 10^{-4}$
0.7812	$8.4321 \times 10^{-5}$	$3.7952 \times 10^{-5}$	$3.7471 \times 10^{-5}$
0.3906	$7.5265 \times 10^{-5}$	$1.0713 \times 10^{-5}$	$9.4435 \times 10^{-6}$

The relative errors  $e_{\check{u}_s}$  and  $e_{\check{u}_p}$  versus  $\delta$  are presented in Fig. 4 for  $h = 8.84$  nm. Regardless of the polarization state of the incident plane wave, the convergence rate of  $e_{\check{u}_q}$  is  $\delta^2$ . Compared to the data in Fig. 2 for the planar backreflector, the shallow rectangular corrugations lower the convergence rate from  $\delta^3$  to  $\delta^2$ . However, the convergence rate of the relative error  $e_{\check{A}_p}$  is of order  $\delta^3$  for the smallest values of  $\delta$ , and that of  $e_{\check{A}_s}$  is faster than  $\delta^2$  but slower than  $\delta^3$ , in Fig. 4.

Table 4: Same as Table 3 but values of the relative errors  $e_{\check{u}_p}$  are shown.

$h$ ( $N_e$ ) $\delta$ (nm)	35.36 (224)	17.68 (896)	8.84 (3584)
12.5	$4.8796 \times 10^{-1}$	$4.7586 \times 10^{-1}$	$4.7932 \times 10^{-1}$
6.25	$1.6456 \times 10^{-1}$	$1.5966 \times 10^{-1}$	$1.5676 \times 10^{-1}$
3.125	$4.4783 \times 10^{-2}$	$4.2526 \times 10^{-2}$	$4.2038 \times 10^{-2}$
1.5625	$1.6742 \times 10^{-2}$	$1.4983 \times 10^{-2}$	$1.4627 \times 10^{-2}$
0.7812	$6.0305 \times 10^{-3}$	$5.1347 \times 10^{-3}$	$4.8565 \times 10^{-3}$
0.3906	$2.5209 \times 10^{-3}$	$1.1464 \times 10^{-3}$	$8.7120 \times 10^{-4}$

The solution  $u^p(x, z)$  from the full model [24] contains strong singularities near the corners of the surface of the metal. Hence, a numerical approximation of the solution will not be as accurate. This issue affects not only the FEM solution  $u_{\delta,2}^{p,h}(x, z)$ , but it also causes a loss of accuracy in the computation of the reference solution  $\check{u}^p(x, z)$ . This suggests that the slightly more erratic behavior of the convergence curve for  $e_{\check{u}_p}$  than of the convergence curve for  $e_{\check{u}_s}$  in Fig. 4 is due to the FEM and not to the approximations introduced by the asymptotic model.

Clearly,  $e_{\check{u}_s} < e_{\check{u}_p}$  in Fig. 4. This also becomes clear from Tables 3 and 4 wherein values of  $e_{\check{u}_s}$  and  $e_{\check{u}_p}$ , respectively, have been stated for several different combinations of  $\delta$  and  $h$ . Whereas  $e_{\check{u}_s} < 1\%$ ,  $e_{\check{u}_p} < 16.5\%$  if  $\delta \leq 6.25$  nm and  $e_{\check{u}_p} < 4.5\%$  if  $\delta \leq 3.125$  nm. Moreover, in both tables, the relative errors do not decrease with  $h$  for the first three values of  $\delta$ , indicating that the asymptotic-model error dominates the FEM error. For  $\delta \leq 0.7812$  nm, there is a value of  $h$  from where the relative error does not significantly change when  $h$  decreases.

In Tables 5 and 6 values of  $e_{\check{A}_s}$  and  $e_{\check{A}_p}$  respectively, have been stated for several different combinations of  $\delta$  and  $h$ , whereas  $e_{\check{A}_s} < 1\%$ ,  $e_{\check{A}_p} < 19.5\%$  if  $\delta \leq 6.25$  nm and  $e_{\check{u}_p} < 7.0\%$  if  $\delta \leq 3.125$  nm. These tables also indicate that  $e_{\check{A}_s} < e_{\check{A}_p}$ , in line with Fig. 4.

Table 5: Same as Table 3 but values of the relative errors  $e_{\tilde{\lambda}_s}$  are shown.

$\lambda_0(N_e)$ $\delta$ (nm)	35.36 (224)	17.68 (896)	8.84 (3584)
12.5	$2.2388 \times 10^{-4}$	$1.9706 \times 10^{-4}$	$1.9077 \times 10^{-4}$
6.25	$2.7147 \times 10^{-6}$	$7.6646 \times 10^{-6}$	$9.5258 \times 10^{-6}$
3.125	$2.6225 \times 10^{-6}$	$3.3044 \times 10^{-6}$	$3.9308 \times 10^{-6}$
1.5625	$4.4622 \times 10^{-6}$	$4.5824 \times 10^{-7}$	$7.6397 \times 10^{-7}$
0.7812	$4.7835 \times 10^{-6}$	$2.3190 \times 10^{-8}$	$2.0315 \times 10^{-7}$
0.3906	$4.8536 \times 10^{-6}$	$8.2720 \times 10^{-8}$	$1.2497 \times 10^{-7}$

Table 6: Same as Table 5 but values of the relative errors  $e_{\tilde{\lambda}_p}$  are shown.

$\lambda_0(N_e)$ $\delta$ (nm)	35.36 (224)	17.68 (896)	8.84 (3584)
12.5	$3.9201 \times 10^{-1}$	$3.8388 \times 10^{-1}$	$3.9209 \times 10^{-1}$
6.25	$1.9463 \times 10^{-1}$	$1.8249 \times 10^{-1}$	$1.7844 \times 10^{-1}$
3.125	$6.8556 \times 10^{-2}$	$5.9692 \times 10^{-2}$	$5.6689 \times 10^{-2}$
1.5625	$2.9210 \times 10^{-2}$	$2.1863 \times 10^{-2}$	$1.9990 \times 10^{-2}$
0.7812	$5.9780 \times 10^{-3}$	$3.7796 \times 10^{-3}$	$1.9480 \times 10^{-3}$
0.3906	$3.0921 \times 10^{-3}$	$8.1344 \times 10^{-4}$	$2.6633 \times 10^{-4}$

### 3.3 Example 3: Periodic Backreflector with Sawtooth Corrugations

In the last example, we consider the backreflector to have sawtooth corrugations described by the function

$$g(x) = \begin{cases} -\delta/2, & 0 \leq x < (1 - \zeta)L/2, \\ \frac{\delta}{\zeta L} \left( \frac{L}{2} - x \right), & (1 - \zeta)L/2 < x < (1 + \zeta)L/2, \\ -\delta/2, & (1 + \zeta)L/2 < x \leq L. \end{cases} \quad (44)$$

All results provided here were calculated with  $\zeta = 0.5$ . When  $\delta = 1.5625$  nm and the incident light is  $s$ -polarized, the absorptances provided by both the full and asymptotic models agree very well. In fact, for this case, the relative error between the full and asymptotic models is at most 1% for any wavelength  $\lambda_0 \in [400, 1000]$  nm. On the other hand, for the  $p$ -polarized incidence case, the relative error was usually less than 5% but could be as high as 15%.

In Fig. 5 we display the values of absorptances, computed with the *asymptotic model*, versus the ratio  $\lambda_0/L$  for different values of  $\delta/L$ , with  $h = 4.42$  nm. These results show that the asymptotic model predicts the absorptance, including resonances, for a shallow sawtooth grating quite well for incident wave of either linear polarization state.

## 4 Conclusions

We have devised an asymptotic model for implementation in the finite element method to calculate electromagnetic diffraction and absorption in planar multilayered structures having a shallow surface-relief grating. Numerical results demonstrate that the model is at least second-order convergent with respect to the thickness  $\delta$  of the grating layer. For incident  $s$ -polarized light, the relative errors of the

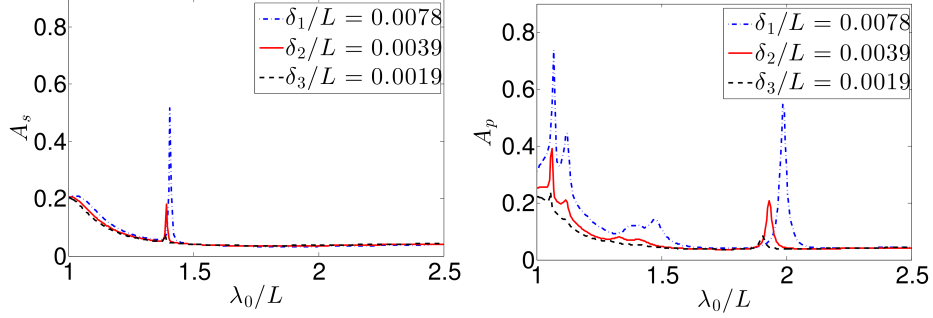


Figure 5: Absorptances  $A_s$  and  $A_p$  versus  $\lambda_0/L$  for  $\delta/L = 0.0078$  (dashed-blue line),  $0.0039$  (solid-red line) and  $0.0019$  (dashed-black line). The mesh size  $h$  of the FEM satisfies  $h/L = 0.011$ . Top panel:  $s$ -polarization. Bottom panel:  $p$ -polarization.

spatially averaged electric field and absorptance are smaller than 1% when  $\delta \leq 12.5$  nm (6.67% of the total height of the structure, and less than 3% of the free-space wavelength). For incident  $p$ -polarized light, lower values of  $\delta$  are needed for the relative errors to have similar magnitudes. These results show that the asymptotic model can be reliably used with FEM to investigate scattering by shallow gratings.

The main advantage of the asymptotic model is that the parameters defining the shallow surface-relief grating are present in the interface parameters and transmission conditions across a planar interface but not in the geometry. FEM calculations are greatly speeded up thereby, as a very fine mesh is not needed for the thin grating layer. This considerably reduces the computational cost of optimizing the grating parameters (e.g., height and duty cycle), since there is no need to change the domain (and, hence, the mesh) at every optimization step.

## Appendix

The asymptotic model can be generalized to case of  $\Gamma = \{\mathbf{r} \in \mathbb{R}^3 : 0 < x < L, |y| < \infty, z = f(x)\}$  being a curved surface instead of a plane, with the surfaces  $\Gamma^\pm$  still defined through Eqs. (2). The generalization is useful for application to a large-amplitude smooth grating perturbed by a thin grating with a smaller period [40].

The domain  $\Omega$  is subdivided into the following three non-overlapping regions:

$$\left. \begin{aligned} \Omega^- &= \{\mathbf{r} \in \mathbb{R}^3 : 0 < x < L, |y| < \infty, -L_m + f(x) - \delta/2 < z < f(x) - \delta/2\} \\ \Omega^\delta &= \{\mathbf{r} \in \mathbb{R}^3 : 0 < x < L, |y| < \infty, f(x) - \delta/2 < z < f(x) + \delta/2\} \\ \Omega^+ &= \{\mathbf{r} \in \mathbb{R}^3 : 0 < x < L, |y| < \infty, f(x) + \delta/2 < z < f(x) + \delta/2 + L_d\} \end{aligned} \right\}. \quad (45)$$

Figure 6 shows an example of the unit cell wherein the surfaces  $\Gamma$  and  $\Gamma^\pm$  are non-planar.

Let us suppose that  $\Gamma$  is parameterized as  $\Gamma = \{(s, f(s)), s \in [0, L]\}$ . Then, the curvature of  $\Gamma$  is defined as

$$C(s) = \left[ 1 + \left( \frac{df(s)}{ds} \right)^2 \right]^{-3/2} \frac{d^2 f(s)}{ds^2} \quad \forall s \in [0, L]. \quad (46)$$

We observe that the boundary-value problem described in Sec. 2 corresponds to  $f(x) = 0$ .

Now, instead of working with the Cartesian coordinate system, we map the point  $(x, z)$  to a point  $(s, \nu)$  in the curvilinear system inspired by the nonplanar  $\Gamma$ . In order to find this mapping, we take  $(s, f(s)) \in \Gamma$ , and denote by  $\hat{\mathbf{u}}_\Gamma(s)$  the normal to  $\Gamma$  at that point. Then, we write  $(s, f(s)) + \nu \hat{\mathbf{u}}_\Gamma(s) = (x(s, \nu), z(s, \nu))$  for  $s \in [0, L]$  and  $\nu \in [-\delta/2, \delta/2]$ . In this case,  $\mathbf{r} = x(s, \nu) \hat{\mathbf{u}}_x + y \hat{\mathbf{u}}_y + z(s, \nu) \hat{\mathbf{u}}_z \in \Omega^\delta$  and the change of

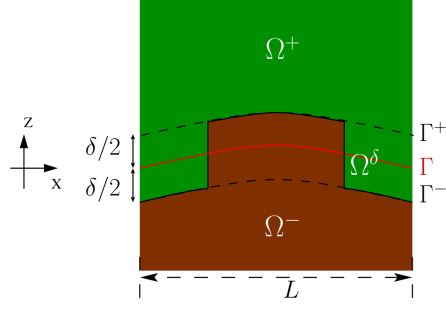


Figure 6: Analogous to Fig. 1 but the surfaces  $\Gamma$ ,  $\Gamma^-$ , and  $\Gamma^+$  are surfaces nonplanar.

variable to scale the domain  $\Omega^\delta$  is  $\xi = \nu/\delta$ . In addition, we need  $u(\mathbf{r} \pm \rho \hat{\mathbf{u}}_\Gamma(s))$  evaluated at  $\mathbf{r} \in \Gamma$  in the limit  $\rho \rightarrow 0$ . The latter function can be obtained using the operator

$$\mathcal{D} = \frac{\frac{\partial}{\partial z} - \frac{df(s)}{ds} \frac{\partial}{\partial s}}{\left[1 + \left(\frac{df(s)}{ds}\right)^2\right]^{1/2}}. \quad (47)$$

We set  $\overline{\varepsilon_r(s)} = \frac{1}{\delta} \int_{-\delta/2}^{\delta/2} \varepsilon_r(x(s, \nu), z(s, \nu)) d\nu$ , and define  $\overline{B^\delta(s)}$  and  $\overline{b^\delta(s)}$  analogously to the quantities defined in Eqs. (25). Hence, writing the differential operators in this curvilinear coordinate system and considering the chain rule for the scaled variable  $\xi$ , equation (22) yields

$$\frac{1}{A(s, \xi)} \frac{\partial}{\partial s} \left( \frac{\overline{B^\delta(s)}}{A(s, \xi)} \frac{\partial \tilde{u}^\delta(s, \xi)}{\partial s} \right) + \frac{\delta^{-2}}{A(s, \xi)} \frac{\partial}{\partial \xi} \left( A(s, \xi) \overline{B^\delta(s)} \frac{\partial \tilde{u}^\delta(s, \xi)}{\partial \xi} \right) + k_0^2 \overline{b^\delta(s)} \tilde{u}^\delta(s, \xi) = 0, \quad \tilde{\mathbf{r}} \in \tilde{\Omega}^\delta, \quad (48)$$

where  $A(s, \xi) = 1 + \delta \xi C(s)$ . Then, for each  $\tilde{\mathbf{r}} \in \tilde{\Omega}^\delta$ , the analog of (29) is

$$\begin{aligned} & \frac{\partial}{\partial \xi} \left( \overline{B^\delta(s)} \frac{\partial \tilde{u}_j^\delta(s, \xi)}{\partial \xi} \right) + \left[ 3\xi C(s) \frac{\partial}{\partial \xi} \left( \overline{B^\delta(s)} \frac{\partial \tilde{u}_{j-1}^\delta(s, \xi)}{\partial \xi} \right) \right. \\ & \left. + C(s) \overline{B^\delta(s)} \frac{\partial \tilde{u}_{j-1}^\delta(s, \xi)}{\partial \xi} \right] + \left[ 3\xi^2 C(s)^2 \frac{\partial}{\partial \xi} \left( \overline{B^\delta(s)} \frac{\partial \tilde{u}_{j-2}^\delta(s, \xi)}{\partial \xi} \right) \right. \\ & \left. + 2\xi C(s)^2 \overline{B^\delta(s)} \frac{\partial \tilde{u}_{j-2}^\delta(s, \xi)}{\partial \xi} + \frac{\partial}{\partial s} \left( \overline{B^\delta(s)} \frac{\partial \tilde{u}_{j-2}^\delta(s, \xi)}{\partial s} \right) \right. \\ & \left. + k_0^2 \overline{b^\delta(s)} \tilde{u}_{j-2}^\delta(s, \xi) \right] + \left[ \xi^3 C(s)^3 \frac{\partial}{\partial \xi} \left( \overline{B^\delta(s)} \frac{\partial \tilde{u}_{j-3}^\delta(s, \xi)}{\partial \xi} \right) \right. \\ & \left. + \xi^2 C(s)^3 \overline{B^\delta(s)} \frac{\partial \tilde{u}_{j-3}^\delta(s, \xi)}{\partial \xi} + \xi C(s) \frac{\partial}{\partial s} \left( \overline{B^\delta(s)} \frac{\partial \tilde{u}_{j-3}^\delta(s, \xi)}{\partial s} \right) \right. \\ & \left. - \xi C'(s) \overline{B^\delta(s)} \frac{\partial \tilde{u}_{j-3}^\delta(s, \xi)}{\partial s} + 3\xi C(s) k_0^2 \overline{b^\delta(s)} \tilde{u}_{j-3}^\delta(s, \xi) \right] \\ & + 3\xi^2 C(s)^2 k_0^2 \overline{b^\delta(s)} \tilde{u}_{j-4}^\delta(s, \xi) + \xi^3 C(s)^3 k_0^2 \overline{b^\delta(s)} \tilde{u}_{j-5}^\delta(s, \xi) = 0, \\ & \tilde{\mathbf{r}} \in \tilde{\Omega}^\delta, \quad j \in \{0, 1, \dots\}. \end{aligned} \quad (49)$$

Moreover, most of the equations grouped as Eqs. (36) remain unchanged, except for

$$\left. \begin{aligned} [B\mathcal{D}\varphi_1](s) &= - \left( \frac{\partial}{\partial s} \left( \overline{B^\delta(s)} \frac{\partial}{\partial s} \right) + k_0^2 \overline{b^\delta(s)} \right) \langle \varphi_0 \rangle(s) - C(s) \langle B\mathcal{D}\varphi_0 \rangle(s), \\ [B\mathcal{D}\varphi_2](s) &= - \left( \frac{\partial}{\partial s} \left( \overline{B^\delta(s)} \frac{\partial}{\partial s} \right) + k_0^2 \overline{b^\delta(s)} \right) \langle \varphi_1 \rangle(s) - C(s) \langle B\mathcal{D}\varphi_1 \rangle(s), \end{aligned} \right\}, \quad (50)$$

$$s \in [0, L],$$

Finally, the transmission conditions for  $u_{\delta,2}^{\pm}$  become

$$\left. \begin{aligned} [u_{\delta,2}](s) &= \delta \left( \overline{B^{\delta}(s)} \right)^{-1} \langle B \mathcal{D}u_{\delta,2} \rangle (s) \\ [B \mathcal{D}u_{\delta,2}](s) &= -\delta \left( \frac{\partial}{\partial s} \left( \overline{B^{\delta}(s)} \frac{\partial}{\partial s} \right) + k_0^2 \overline{b^{\delta}(s)} \right) \langle u_{\delta,2} \rangle (s) - \delta C(s) \langle \mathcal{D}u_{\delta,2} \rangle (s) \end{aligned} \right\},$$

$$s \in [0, L]. \quad (51)$$

Clearly, Eqs. (27), (36)<sub>4</sub>, (36)<sub>6</sub>, and (39a) are simplifications for the foregoing equations for planar  $\Gamma$  (i.e.,  $C(s) = 0 \forall s \in [0, L]$ ).

## Acknowledgment

M. E. Solano is partially supported by CONICYT–Chile through the FONDECYT project No. 1160320. R. Rodríguez and M. E. Solano are partially supported by BASAL project, CMM, Universidad de Chile. C. Rivas acknowledges the support of the Scholarship Program of CONICYT–Chile. A. Lakhtakia thanks the Charles Godfrey Binder Endowment at the Pennsylvania State University for ongoing support of his research, with partial funding from US NSF grant number DMS-1619901. The research of P. B. Monk is partially supported by US NSF grant number DMS-1619904.

## References

- [1] G. Floquet, "Sur les équations différentielles linéaires à coefficients périodiques," *Annales de l'École Normale Supérieure* **12**, 47–88 (1883).
- [2] F. Bloch, "Über die Quantenmechanik der Elektronen in Kristallgittern," *Z. Phys.* **52**, 555–600 (1929).
- [3] P. C. Waterman, "Scattering by periodic surfaces," *J. Acoust. Soc. Am.* **57**, 791–802 (1975).
- [4] D. Maystre (Ed.), *Selected Papers on Diffraction Gratings* (SPIE Press, 1993).
- [5] J. A. Polo Jr., T. G. Mackay, and A. Lakhtakia, *Electromagnetic Surface Waves: A Modern Perspective*, (Elsevier, 2013).
- [6] E. G. Loewen and E. Popov, *Diffraction Gratings and Applications* (Marcel Dekker, 1997).
- [7] J. Homola, I. Koudela, and S. S. Yee, "Surface plasmon resonance sensors based on diffraction gratings and prism couplers: sensitivity comparison," *Sens. Actuat. B: Chem.* **54**, 16–24 (1999).
- [8] P. Sheng, A. N. Bloch, and R. S. Stepleman, "Wavelength-selective absorption enhancement in thin-film solar cells," *Appl. Phys. Lett.* **43**, 579–581 (1983).
- [9] M. Solano, M. Faryad, A. S. Hall, T. E. Mallouk, P. B. Monk, and A. Lakhtakia, "Optimization of the absorption efficiency of an amorphous-silicon thin-film tandem solar cell backed by a metallic surface-relief grating," *Appl. Opt.* **52**, 966–979 (2013).
- [10] A. S. Hall, M. Faryad, G. D. Barber, L. Liu, S. Erten, T. S. Mayer, A. Lakhtakia, and T. E. Mallouk, "Broadband light absorption with multiple surface plasmon polariton waves excited at the interface of a metallic grating and photonic crystal," *ACS Nano* **7**, 4995–5007 (2013).
- [11] D. P. Nicholls, S.-H. Oh, T. W. Johnson, and F. Reitich, "Launching surface plasmon waves via vanishingly small periodic gratings," *J. Opt. Soc. Am. A* **33**, 276–285 (2016).

- [12] M. E. Solano, G. D. Barber, A. Lakhtakia, M. Faryad, P. B. Monk, and T. E. Mallouk, "Buffer layer between a planar optical concentrator and a solar cell," *AIP Adv.* **5**, 097150 (2015).
- [13] B. Gralak, "Exact modal methods," in: E. Popov, Ed., *Gratings: Theory and Numeric Applications*, (Institut Fresnel, CNRS, Université d'Aix-Marseille, 2012). Available at <http://www.fresnel.fr/files/gratings/Chapter10.pdf> (accessed 19 April 2016).
- [14] A. Taflove and S. C. Hagness, *Computational Electrodynamics: The Finite-Difference Time-Domain Method, 3rd ed.* (Artech House, 2005).
- [15] H. Ichikawa, "Electromagnetic analysis of diffraction gratings by the finite-difference time-domain method," *J. Opt. Soc. Am. A* **15**, 152–157 (1998).
- [16] V. Jandhyala, D. Sengupta, B. Shanker, E. Michielssen, M. Feng, and G. Stillman, "Efficient electromagnetic analysis of two-dimensional finite quasi-random gratings for quantum well infrared photodetectors," *J. Appl. Phys.* **83**, 3360–3363 (1998).
- [17] T. Oğuzer and F. Kuyucuoğlu, "Method of moments solution by using sinc-type basis functions for the scattering from a finite number of conducting strip gratings," *Turk. J. Elec. Eng.* **16**, 95–109 (2008).
- [18] G. Granet, L. B. Andriamanampisoa, K. Raniriharinosy, A. M. Armeanu, and K. Edee, "Modal analysis of lamellar gratings using the moment method with subsectional basis and adaptive spatial resolution," *J. Opt. Soc. Am. A* **27**, 1303–1310 (2010).
- [19] N. Chateau and J.-P. Hugonin, "Algorithm for the rigorous coupled-wave analysis of grating diffraction," *J. Opt. Soc. Am. A* **11**, 1321–1331 (1994).
- [20] M. G. Moharam, E. B. Grann, and D. A. Pommet, "Formulation for stable and efficient implementation of the rigorous coupled-wave analysis of binary gratings," *J. Opt. Soc. Am. A* **12**, 1068–1076 (1995).
- [21] G. Granet and B. Guizal, "Efficient implementation of the coupled-wave method for metallic lamellar gratings in TM polarization," *J. Opt. Soc. Am. A* **13**, 1019–1023 (1996).
- [22] P. Lalanne and G. M. Morris, "Highly improved convergence of the coupled-wave method for TM polarization," *J. Opt. Soc. Am. A* **13**, 779–784 (1996).
- [23] P. B. Monk, *Finite Element Methods for Maxwell's Equations* (Oxford University Press, 2003).
- [24] M. E. Solano, M. Faryad, A. Lakhtakia, and P. B. Monk, "Comparison of rigorous coupled-wave approach and finite element method for photovoltaic devices with periodically corrugated metallic back reflector," *J. Opt. Soc. Am. A* **31**, 2275–2284 (2014).
- [25] M. V. Shuba, M. Faryad, M. E. Solano, P. B. Monk and A. Lakhtakia, "Adequacy of the rigorous coupled-wave approach for thin-film silicon solar cells with periodically corrugated metallic backreflectors: spectral analysis," *J. Opt. Soc. Am. A* **32**, 1222–1230 (2015).
- [26] Lord Rayleigh, "On the dynamical theory of gratings," *Proc. R. Soc. Lond. A* **79**, 399–415 (1907).
- [27] R. F. Millar, "The Rayleigh hypothesis and a related least-squares solution to scattering problems for periodic surfaces and other scatterers," *Radio Sci.* **8**, 785–796 (1973).
- [28] A. Lakhtakia, V. K. Varadan, and V. V. Varadan, "A T-matrix approach for EM scattering by a perfectly conducting periodic surface," *Proc. IEEE* **73**, 1238–1239 (1985).

- [29] J. Wauer and T. Rother, "Considerations to Rayleigh's hypothesis," *Opt. Commun.* **282**, 339–350 (2009).
- [30] J. Chandezon, M. T. Dupuis, and G. Cornet, "Multicoated gratings: a differential formalism applicable in the entire optical region," *J. Opt. Soc. Am. A* **72**, 839–846.
- [31] L. Li, J. Chandezon, G. Granet, and J. P. Plumey, "Rigorous and efficient grating-analysis method made easy for optical engineers," *Appl. Opt.* **38**, 304–313 (1999).
- [32] L. Li, "Oblique-coordinate-system-based Chandezon method for modeling one-dimensionally periodic, multilayer, inhomogeneous, anisotropic gratings," *J. Opt. Soc. Am. A* **16**, 2521–2531 (1999).
- [33] M. E. Inchaussandague and R. A. Depine, "Rigorous vector theory for diffraction gratings made of biaxial crystals," *J. Mod. Opt.* **44**, 1–27 (1997).
- [34] R. A. Depine, M. E. Inchaussandague, and A. Lakhtakia, "Vector theory of diffraction by gratings made of a uniaxial dielectric-magnetic material exhibiting negative refraction," *J. Opt. Soc. Am. B* **23**, 514–528 (2006).
- [35] B. Delourme, H. Haddar, and P. Joly, "Approximate models for wave propagation across thin periodic interfaces," *J. Math. Pures Appl.* **98**, 28–71 (2012).
- [36] B. Delourme, H. Haddar, and P. Joly, "On the well-posedness, stability and accuracy of an asymptotic model for thin periodic interfaces in electromagnetic scattering problems," *Math. Models Methods Appl. Sci.* **23**, 2433–2464 (2013).
- [37] B. Delourme, "High-order asymptotics for the electromagnetic scattering by thin periodic layers," *Math. Methods Appl. Sci.* **38**, 811–833 (2015).
- [38] Ö. Özdemir, H. Haddar, and A. Yaka, "Reconstruction of the electromagnetic field in layered media using the concept of approximate transmission conditions," *IEEE Trans. Antennas Propagat.* **59**, 2964–2972 (2011).
- [39] A. Maurel, J.-J. Marigo, and A. Ourir, "Homogenization of ultrathin metallo-dielectric structures leading to transmission conditions at an equivalent interface," *J. Opt. Soc. Am. B* **33**, 947–956 (2016).
- [40] A. Lakhtakia, V. K. Varadan, and V. V. Varadan, "Scalar scattering characteristics of a periodic, impenetrable surface: Effect of surface modeling errors," *J. Appl. Phys.* **60**, 4090–4094 (1986).
- [41] M. Faryad, A. S. Hall, G. D. Barber, T. E. Mallouk, and A. Lakhtakia, "Excitation of multiple surface-plasmon-polariton waves guided by the periodically corrugated interface of a metal and a periodic multilayered isotropic dielectric material," *J. Opt. Soc. Am. B* **29**, 704–713 (2012).
- [42] M. Born and E. Wolf, *Principles of Optics*, 6th ed. (Cambridge University, 1980), Sect. 1.6.
- [43] S. C. Brenner and L. R. Scott, *The Mathematical Theory of Finite Element Methods, 2nd ed.* (Springer, 2002).

# Centro de Investigación en Ingeniería Matemática (CI<sup>2</sup>MA)

## PRE-PUBLICACIONES 2016

- 2016-11 GABRIEL N. GATICA, RICARDO RUIZ-BAIER, GIORDANO TIERRA: *A posteriori error analysis of an augmented mixed method for the Navier-Stokes equations with nonlinear viscosity*
- 2016-12 MANUEL SOLANO, FELIPE VARGAS: *A high order HDG method for Stokes flow in curved domains*
- 2016-13 HUANGXIN CHEN, WEIFENG QIU, KE SHI, MANUEL SOLANO: *A superconvergent HDG method for the Maxwell equations*
- 2016-14 LOURENCO BEIRAO-DA-VEIGA, DAVID MORA, GONZALO RIVERA: *A virtual element method for Reissner-Mindlin plates*
- 2016-15 RODOLFO ARAYA, CHRISTOPHER HARDER, ABNER POZA, FREDERIC VALENTIN: *Multiscale hybrid-mixed method for the Stokes and Brinkman equations - The method*
- 2016-16 LUIS M. CASTRO, JOSÉ GONZÁLEZ, VÍCTOR H. LACHOS, ALEXANDRE PATRIOTA: *A confidence set analysis for observed samples: A fuzzy set approach*
- 2016-17 RAIMUND BÜRGER, STEFAN DIEHL, CAMILO MEJÍAS: *A model of continuous sedimentation with compression and reactions*
- 2016-18 CARLOS GARCIA, GABRIEL N. GATICA, SALIM MEDDAHI: *Finite element analysis of a pressure-stress formulation for the time-domain fluid-structure interaction problem*
- 2016-19 ANAHI GAJARDO, BENJAMIN HELLOUIN, DIEGO MALDONADO, ANDRES MOREIRA: *Nontrivial turmites are Turing-universal*
- 2016-20 LEONARDO E. FIGUEROA: *Error in Sobolev norms of orthogonal projection onto polynomials in the unit ball*
- 2016-21 RAIMUND BÜRGER, JULIO CAREAGA, STEFAN DIEHL: *Entropy solutions of a scalar conservation law modelling sedimentation in vessels with varying cross-sectional area*
- 2016-22 AKHLESH LAKHTAKIA, PETER MONK, CINTHYA RIVAS, RODOLFO RODRÍGUEZ, MANUEL SOLANO: *Asymptotic model for finite-element calculations of diffraction by shallow metallic surface-relief gratings*

Para obtener copias de las Pre-Publicaciones, escribir o llamar a: DIRECTOR, CENTRO DE INVESTIGACIÓN EN INGENIERÍA MATEMÁTICA, UNIVERSIDAD DE CONCEPCIÓN, CASILLA 160-C, CONCEPCIÓN, CHILE, TEL.: 41-2661324, o bien, visitar la página web del centro: <http://www.ci2ma.udec.cl>



**CENTRO DE INVESTIGACIÓN EN  
INGENIERÍA MATEMÁTICA (CI<sup>2</sup>MA)  
Universidad de Concepción**



Casilla 160-C, Concepción, Chile  
Tel.: 56-41-2661324/2661554/2661316  
<http://www.ci2ma.udec.cl>



---